Article

# Digital Imaging for Online Monitoring and Control of Industrial Snack Food Processes

Honglu Yu, John F. MacGregor, Gabe Haarsma, and Wilfred Bourg

*Ind. Eng. Chem. Res.*, **2003**, 42 (13), 3036-3044• DOI: 10.1021/ie020941f • Publication Date (Web): 20 May 2003

# Digital Imaging for Online Monitoring and Control of Industrial Snack Food Processes

**Honglu Yu and John F. MacGregor***

*McMaster Advanced Control Consortium, Department of Chemical Engineering, McMaster University, Hamilton, Ontario L8S 4L7, Canada*

**Gabe Haarsma† and Wilfred Bourg**

*Frito-Lay Technology R&D, Frito-Lay, Inc., P.O. Box 660634, Dallas, Texas 75266-0634*

Results from the implementation of an online color imaging system on industrial snack food production lines are presented. Feature information is extracted from images using multivariate image analysis based on principal component analysis and is used to develop models to predict the coating content and the coating distribution on the products. The imaging system is used to monitor these product quality variables and to detect and diagnose operational problems in the plants. It is also used to directly implement closed-loop feedback control over the coating concentration.

## 1. Introduction

The availability of informative, inexpensive, and robust online sensors is one of the most important factors for the successful monitoring and control of processes. The petrochemical industry made rapid advances in multivariable model predictive control largely because they had the availability and abundance of inexpensive and informative sensors such as thermocouples, pressure transducers, flowmeters, pH and ion-specific meters, and gas chromatographs. This is a direct result of the fact that the major streams in petrochemical processes consist of well-mixed gases and liquids, which made the use of such sensors very easy. On the other hand, the solids processing industry has had much less success at implementing advanced control precisely because of the lack of such sensors. However, with the advent of inexpensive digital cameras over the past decade, things are changing rapidly. Today an RGB (red, green, and blue) color camera connected to a fairly powerful PC is on the order of only a few thousand dollars or so. In contrast, to insert a simple thermocouple well into a process line or a reactor is considerably more expensive. If affordable digital imaging systems can be used to effectively extract subtle information on the behavior of a process or on the quality of the product, then it could indeed lead to a more rapid application of advanced control in process industries manufacturing of solid products such as pulp and paper, polymer sheet and films, and food products. In this paper we report on the development of such an online imaging system and its use for the online monitoring and feedback control of product quality variables in the snack food industry.

Much of the literature on digital image processing involves methods for altering the visual image in some way in order to make it more visually appealing or to extract information on the shapes, boundaries, or location of various observable features. In this sense, traditional image processing techniques[1−3] serve as automated vision systems performing operations faster and more precisely than human operators. These are indeed a very important class of problems. However, many quality monitoring and control problems are more similar to those treated in this paper. They do not involve image enhancement issues but rather the extraction of subtle information from the image (much of which is not readily visible to the human eye) that is related to product quality. For example, in this paper we are concerned with the prediction of the average coating concentrations and the distribution of the coating on snack food products passing on a moving belt under the imaging system. In these situations, image processing is not concerned with image enhancement or even with the image space at all. Rather, the problem is one of information extraction from the image and the use of such information for prediction, monitoring, and control. For this purpose a different set of techniques falling under the heading of multivariate image analysis (MIA),[4−6] which employs multivariate statistical techniques such as principal component analysis (PCA) and partial least squares (PLS), have been developed. In this approach, most of the analysis is done in the latent variable feature space rather than in the image space. Although most of the MIA methods have been applied to the analysis of single still images, an indication of their potential for monitoring time-varying images was presented by Bharati and MacGregor[7] and subsequently applied to the online monitoring of lumber defects[8] and pulp and paper quality.[8] In Yu and MacGregor,[9] several MIA and multivariate image regression techniques for the extraction of the coating content and distribution from time-varying images of snack food products were developed. The most robust of those methods is used in this paper for the online monitoring and control of these snack food product lines.

The paper is organized as follows. Following some general background on digital images and on MIA, an overview of the methodology used for the prediction of

* To whom correspondence should be addressed. Tel.: (905)-525-9140 ext. 24951. Fax: (905)521-1350. E-mail: macgreg@mcmaster.ca.

† Present address: Westhollow Technology Center, Shell Global Solutions (U.S.) Inc., Houston, TX 77082-3102.

10.1021/ie020941f CCC: $25.00 
Published on Web 05/20/2003

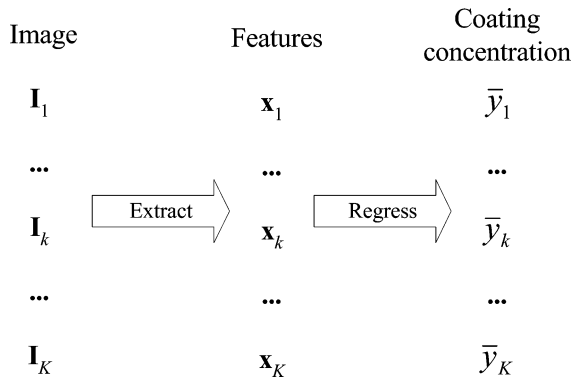


**Figure 1.** Scheme of the model developing procedure.

the coating concentration and distribution is presented. Online results of using this methodology are then shown for two different product lines. Preliminary trial results are first shown to illustrate the power of the approach for monitoring and fault detection and for tracking the coating concentration over a series of manipulated variable changes. Online results from the commissioned system are then presented to show its ability to predict the coating concentration and distribution under a series of process changes and to show its direct use in closed-loop control of the coating concentration.

## 2. Background

**2.1. Color Image Data.** In the most commonly used electronic cameras, the color of each pixel is characterized by the numerical values (normally integers from 0 to 255) of its RGB channels. Therefore, a color image can be expressed as a three-way matrix. Two ways are the spatial coordinates, and the third way is the color channel. Without considering the spatial coordinates of the pixels, we can unfold the image matrix and express it as a two-way matrix.

$$\boldsymbol{I}_{N_{row}\times N_{col}\times 3} \xrightarrow{\text{unfold}} \mathbf{I}_{N\times 3} = \begin{bmatrix} c_{1,\mathrm{r}} & c_{1,\mathrm{g}} & c_{1,\mathrm{b}} \\ \vdots & \vdots & \vdots \\ c_{i,\mathrm{r}} & c_{i,\mathrm{g}} & c_{i,\mathrm{b}} \\ \vdots & \vdots & \vdots \\ c_{N,\mathrm{r}} & c_{N,\mathrm{g}} & c_{N,\mathrm{b}} \end{bmatrix} = \begin{bmatrix} \mathbf{c}_1 \\ \vdots \\ \mathbf{c}_i \\ \vdots \\ \mathbf{c}_N \end{bmatrix}$$

$\boldsymbol{I}$ is a three-way image matrix with image size $N_{\mathrm{row}} \times N_{\mathrm{col}}$ and three color channels. $\mathbf{I}$ is the unfolded two-way image matrix. $N$ is the number of pixels in the image, $N = N_{\mathrm{row}} \times N_{\mathrm{col}}$. $c_{i,\mathrm{r}}$, $c_{i,\mathrm{g}}$, and $c_{i,\mathrm{b}}$ ($i = 1, ..., N$) are the intensity values of channels R, G, and B for pixel $i$. $\mathbf{c}_i$ ($i = 1, ..., N$) is the $i$th row vector of $\mathbf{I}$, which represents the color value of pixel $i$. In the following text, we always use the two-way matrix $\mathbf{I}$ to represent an image.

**2.2. Problem Definition and Solution Strategy.** Let us consider a data set of $K$ color images $\mathbf{I}_K$ and the corresponding $K$ laboratory-analyzed average coating concentrations $\bar{y}_k$ ($k = 1, ..., K$). A model to predict the coating concentration can be obtained by regressing features extracted from the images against the corresponding average coating concentrations. In this paper, PLS regression is employed because of the high correlation among the feature variables. Figure 1 shows the model development procedure.

Feature extraction is a critical step to achieve good prediction results. In Yu and MacGregor,[9] six feature extraction methods (including two overall feature methods and four distribution feature methods) are compared and discussed. Examples show that, for prediction of the average coating level of the whole image, all six methods can achieve good results. However, when the coating level from small subimages is predicted, only one method (method 6[9]) exhibits sufficient robustness in prediction. Therefore, in this paper, only this method, which is a method that converts the image into a one-dimensional cumulative histogram, is used to build the model.

**2.3. Multiway PCA (MPCA).** A color image is a multivariate image composed of three variables (R, G, and B channels). In this paper, the method is developed using MIA techniques,[4,5,6] which are based on MPCA.

MPCA is equivalent to performing PCA on the unfolded image matrix $\mathbf{I}$ to yield

$$\mathbf{I} = \sum_{a=1}^{A} \mathbf{t}_a \mathbf{p}_a{}^{\mathrm{T}}$$

where $A$ is the number of principal components, $\mathbf{t}$ is the score vector, and $\mathbf{p}$ is the loading vector.

Because the row dimension of the $\mathbf{I}$ matrix is very large (equal to 307 200 for a 480 × 640 image) and the column dimension is much smaller (equal to 3 for an RGB color image), a kernel algorithm[6] is used to compute the PCA loading and score vectors. In this algorithm, the kernel matrix ($\mathbf{I}^{\mathrm{T}}\mathbf{I}$) is first formed, and then singular value decomposition is performed on this very low dimensional matrix (3 × 3 for RGB color images) to obtain loading vectors $\mathbf{p}_a$ ($a = 1, ..., A$). When there is more than one image being considered, the kernel matrix is calculated as $\sum_k \mathbf{I}_k{}^{\mathrm{T}}\mathbf{I}_k$. After loading vectors are obtained, the corresponding score vectors $\mathbf{t}_a$ are then computed via $\mathbf{t}_a = \mathbf{I}\mathbf{p}_a$. Because the first two components normally explain most of the variance, instead of working in the original three-dimensional RGB space, working in the two-dimensional orthogonal $t_1$−$t_2$ score space allows us interpret the image much easier.

The scatter score plot ($t_2$ vs $t_1$) is an important tool in MIA. Because similar colors in the original image will yield almost identical ($t_1$, $t_2$) score combinations, many points overlap in this scatter plot. Following Geladi and Grahn,[6] the score plot ($t_2$ vs $t_1$) is then constructed as a two-dimensional histogram with a grid of 256 × 256 bins.

## 3. Procedure for Predicting the Coating Concentration and Coating Distribution

**3.1. Training Data Sets.** During building of a model, the first step is to collect an adequate set of training data. A successful model requires a set of sample images including both noncoated and coated product samples with varied coating levels. For each coated product image, the corresponding average coating is obtained by laboratory analysis of the product. In this paper, models are built for two types of snack food. All of the images are collected from the online camera system, and grab samples corresponding to those images are taken to the laboratory for analysis. The images are all 480 × 640 RGB color images, with 256 intensity levels in each channel. Some sample images are shown in Figure 2. Details on the size of the training and test sets for each product can be found in Table 1. In the following

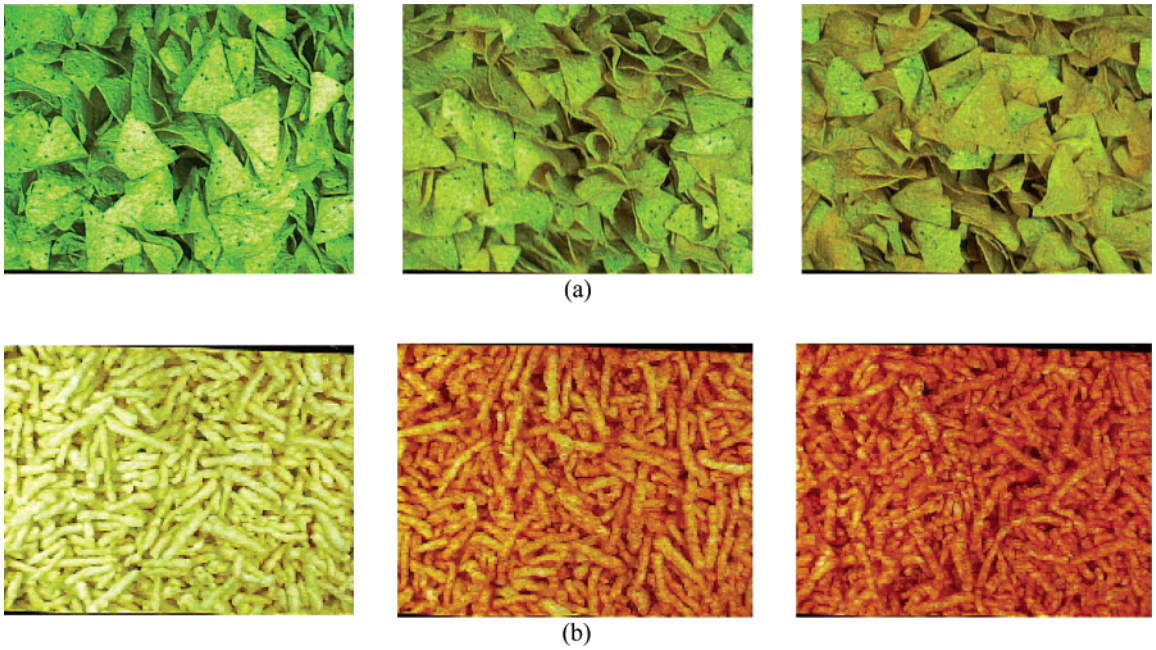


**Figure 2.** Sample images for two products: (a) product A; (b) product B. For each row from left to right are noncoated product image, low-coated product image, and high-coated product image.

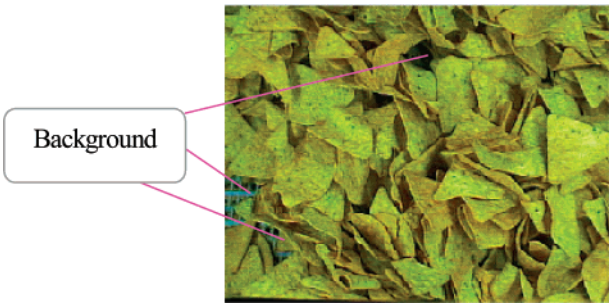


**Figure 3.** Background consisting of an exposed conveyor belt.

**Table 1. Samples Images for Two Products**

| product | comments |
|---|---|
| A | 110 samples: 55 for training and 55 for test |
| B | 180 samples: 90 for training and 90 for test |

algorithm section, we use product A as the basis for illustrating the methodology.

**3.2. Image Preprocessing: Removing Background Pixels.** One important step before feature extraction is background removal. In this online application, background mainly arises from exposed sections of the conveyor belt (see Figure 3).

Detecting and eliminating these background pixels through traditional image analysis methods performed by operations directly in the image space itself can be very difficult and time-consuming. Working in the space of the scatter plots of the PCA scores concentrates all of the background pixels in one region and allows for easy removal through a masking operation in this space. In this approach, the score vectors ($t_1$ and $t_2$) from a PCA (without mean-centering) are computed using all of the training images and a *pure belt image*. As in traditional MIA techniques,[4,6,7] masks are chosen in the $t_1-t_2$ score space to separate different features (in this case the background from the product).

However, instead of the iterative trial-and-error approach commonly used in MIA to determine these mask boundaries, a more quantitative approach[9] is used. The

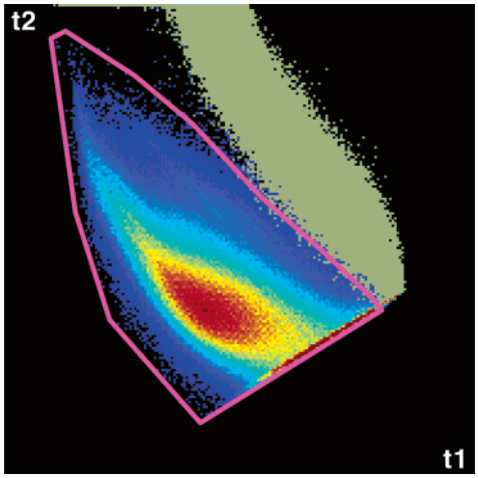


**Figure 4.** Selection of a product mask in the $t_1-t_2$ score space. The middle colorful part represents a color-coded covariance plot (cold colors represent small covariance values with spicy content, and warm colors represent large values). Gray-green pixels show the location of the belt image. The purple polygon is the product mask. Pixels falling outside the mask are deemed to be background.

approach can be briefly summarized as follows. The $t_1-t_2$ score plots for each image obtained from the PCA are stacked together with their corresponding average coating concentrations. The covariance between the number of pixels in each bin of the $t_1-t_2$ histograms and the average coating concentrations is calculated. A covariance plot in the $t_1-t_2$ space as shown in Figure 4 is constructed that reflects the relation of the histogram counts at each of the ($t_1$, $t_2$) combinations with the coating level. Because the background is independent of the coating concentration, histogram counts corresponding to a background color should have low values in the covariance plots. Moreover, the projection of the pure belt image into the $t_1-t_2$ space (shown as gray-green pixels in Figure 4) can also help to locate belt pixels. A product mask can then be selected (the area within the purple polygon in Figure 4) based on the

covariance information and on the location of the belt image projection. For each new image, score pixels falling outside the product mask are considered to belong to the background. It has been shown[9] that this technique is able to remove not only the usual background feature (conveyor belt) but also the unexpected background (fingers of the operator in the example).

**3.3. Feature Extraction.** As mentioned earlier, feature extraction from the image is the key step in building a good model. In work by Yu and MacGregor,[9] several different feature extraction methods were used and compared. In this paper, we use one of the distribution feature methods that is briefly discussed in this section.

The color of a pixel is a function of both the local coating concentration and other imaging conditions (such as lighting). Although pixels containing the same amount of coating concentration may exhibit variations in colors, it is reasonable to assume that pixels having the same color contain the same amount of coating. For an image, the number of pixels, whose color is [*r*, *g*, *b*] (*r*, *g*, and *b* are integer values ranging from 0 to 255), can be counted as $n_{[r,g,b]}$. If the coating concentration for each of these pixels is $y_{[r,g,b]}$, then the average coating concentration for the whole image can be calculated as

$$\bar{y} = \sum_r \sum_g \sum_b y_{[r,g,b]} \frac{n_{[r,g,b]}}{N} \qquad r, g, b = 0, 1, ..., 255 \quad (1)$$

Notice that eq 1 has a linear model structure. For each image, $n_{[r,g,b]}/N$ is a 256 × 256 × 256 three-dimensional relative histogram and can be used as a high-dimensional feature variable. Estimation of $y_{[r,g,b]}$ can be obtained through a linear regression between $n_{[r,g,b]}/N$ and the average coating concentration using the model in eq 1. However, this model is neither robust nor practical because obtaining such a three-dimensional histogram for each image is time-consuming and, even if the three-dimensional histogram is computed, a large number ($256^3 = 16\,777\,216$) of feature variables have low signal-to-noise ratios, leading to poor estimation of the model parameters.

To reduce the number of feature variables, the color space can be divided into *L* classes, such that pixels falling in a class contain a similar amount of coating. In this form, each class becomes a new histogram bin and the average coating concentration for an image can be obtained by

$$\bar{y} \approx \sum_{j=1}^{L} y_j \frac{n_j}{N} \quad (2)$$

where $n_j$ and $y_j$ are the pixels and the average coating concentration belonging to class *j*.

The model structure remains linear as long as the assumption that pixels in the same class represent a similar amount of coating is not strongly violated.

In this paper, the method we use for classifying the color space[9] starts with a fine (256 × 256) histogram in the $t_1$−$t_2$ color space and then lumps the points in that space into histogram bins that are expected to contain similar values of the coating concentration. Unlike the PCA performed in the background removing step, here PCA is performed on the images corrected by subtracting the average color of noncoated product images because we would like to obtain a model that captures most of the difference between coated and noncoated products. To define histogram bin classes in the score spaces that contain pixels having similar coating content, two covariance plots are computed as was done in the background removal step. Covariance plots are computed between the counts in the histogram bins and two variables, $\mathbf{z}_1$ and $\mathbf{z}_2$, related to the average coating concentrations in the images.

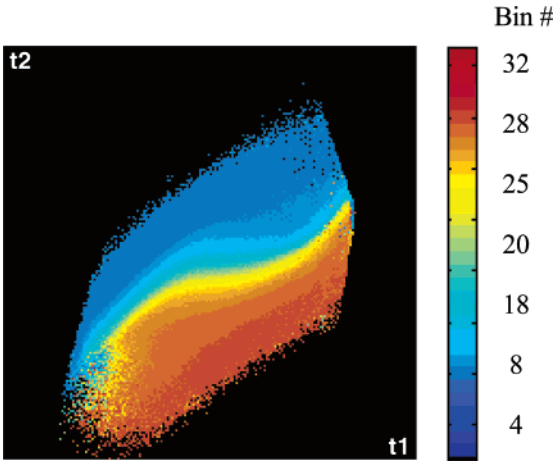


**Figure 5.** Color-coded angle plot in the $t_1$−$t_2$ space, with 32 bins based on angle values. Image pixels having ($t_1$, $t_2$) values falling within the same bin should have similar coating levels.

$$\mathbf{z}_1 = \begin{bmatrix} \bar{y}_{I_1} \\ \bar{y}_{I_2} \\ \vdots \\ \bar{y}_{I_K} \end{bmatrix}, \quad \mathbf{z}_2 = |\mathbf{z}_1 - y^*| = \begin{bmatrix} |\bar{y}_{I_1} - y^*| \\ |\bar{y}_{I_2} - y^*| \\ \vdots \\ |\bar{y}_{I_K} - y^*| \end{bmatrix},$$

$$y^* = \frac{\max(\bar{y}) + \min(\bar{y})}{2}$$

Two covariance plots were necessary in order to obtain a unique or one-to-one correspondence between the bin classes and coating content.[9] For each ($t_1$, $t_2$) location, a phase angle can be computed for the observed point in the space of the two covariance values. Therefore, an angle plot can be obtained in which similar angle values indicate similar coating contents. Figure 5 is the color-coded angle plot in the $t_1$−$t_2$ space. A total of 32 bins are selected based on angle values. Then, a one-dimensional histogram can be formed for each image by counting the number of pixels falling in each bin. The final feature variables are chosen as the 32 values of the cumulative histogram.[9]

**3.4. PLS Model To Predict the Coating Concentration.** Once the feature variables have been obtained, we can build inferential models by regressing these feature variables against the laboratory coating concentration for the training set. PLS regression is used because the feature data are highly correlated and because it allows for validation of data from new images.

After the PLS model was obtained using the training data set, the prediction performance of the model was evaluated against the test data sets (Table 1). Figure 6 plots the predicted average coating level vs the laboratory analysis data for product A. The fit of the training data is very good, and the prediction of the new test data is almost equally good.

To obtain a prediction for each new image, we first preprocess the image to remove any background pixels.

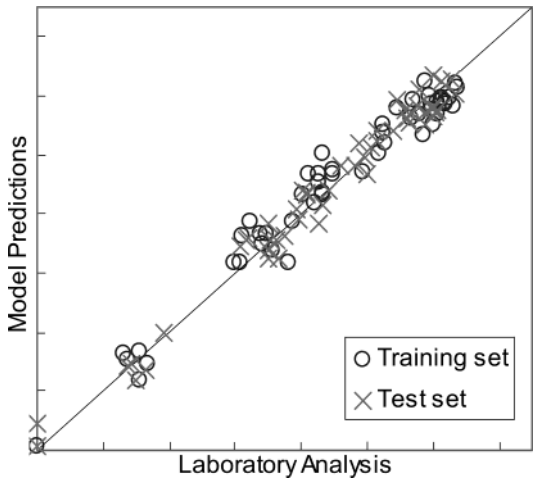


**Figure 6.** Predicted vs observed coating content.

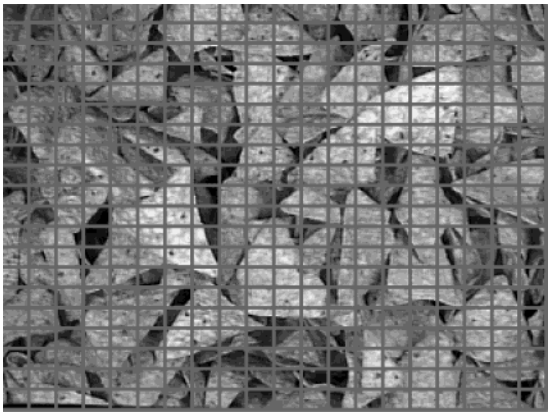

**Figure 7.** Image divided into 20 × 20 windows.

This is done by projecting the color value of the pixels onto the $t_1-t_2$ plane obtained by the first PCA model (section 3.2) and then removing the pixels falling outside the product mask (see Figure 4). After removal of the background, the remaining product pixels are projected onto the $t_1-t_2$ plane obtained by the second PCA model (section 3.3). By counting the number of pixels falling into each of the bins (Figure 5), we obtain the 32-bin cumulative one-dimensional histogram to be used as regressor variables in the PLS model. The average coating level is then predicted by the PLS model.

**3.5. Estimation of the Coating Distribution.** The method developed above is almost independent of the image size.[9] Therefore, the coating distribution can be estimated by a small window strategy.[9] In this small window strategy, the image is divided into many small pieces (see Figure 7), and the coating distribution is obtained by calculating the average coating concentration for each subimage. Variance of the coating distribution can be estimated from this distribution and used for online monitoring. See work by Yu and MacGregor [9] for further details on this and other approaches for estimating the coating distribution.

## 4. Results

**4.1. Snack Food Processing.** Most snack foods typically are produced by coating the base product with flavored coating. The coating plays an important role in both the flavor and the appearance of a snack and greatly influences its acceptability. The usual procedure of taking infrequent samples and analyzing them for the coating concentration in the laboratory gives no information on anything except long-term trends and no information on the coating distribution. Furthermore, it is a time-consuming and expensive procedure. Clearly, there is a tremendous opportunity for an online imaging system.

A schematic of the processes and the imaging systems is shown in Figure 8. Coated and uncoated products are mixed in a tumbler, and then the coated product is conveyed via a moving belt to the subsequent operations. An RGB camera and lighting system is mounted above the moving belt and images are sent to a computer through a frame grabber. The choice of the sampling interval depends on the objectives for each process. The time required for processing one image was less than a second.

Results are now presented to illustrate the abilities of the system. The first two examples provide an assessment of the system's potential to track the coating concentration online under different conditions. They represent results obtained on the first day of implementation of the image processing algorithm. The subsequent studies illustrate typical results from using the system for routine monitoring and closed-loop control over the past year.

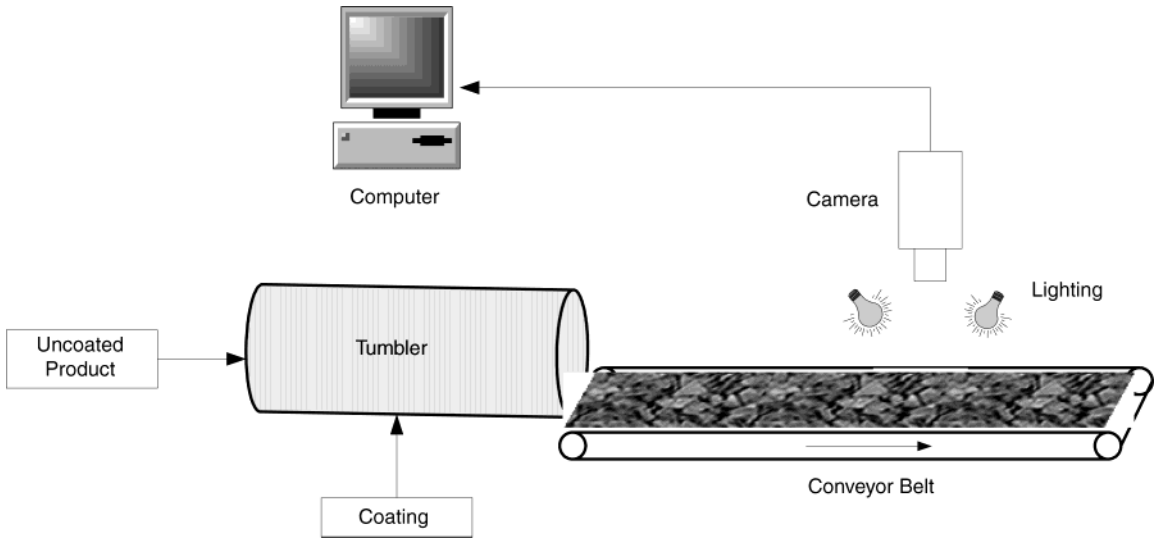


**Figure 8.** Schematic of the processes and imaging systems.

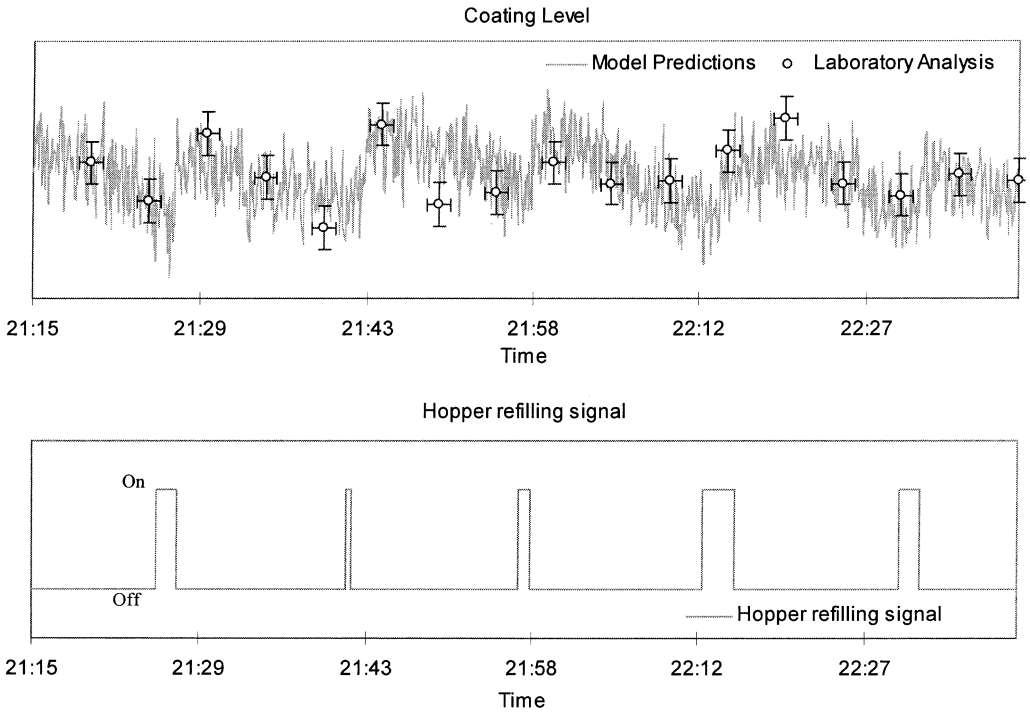


**Figure 9.** Detection of the hopper effect.

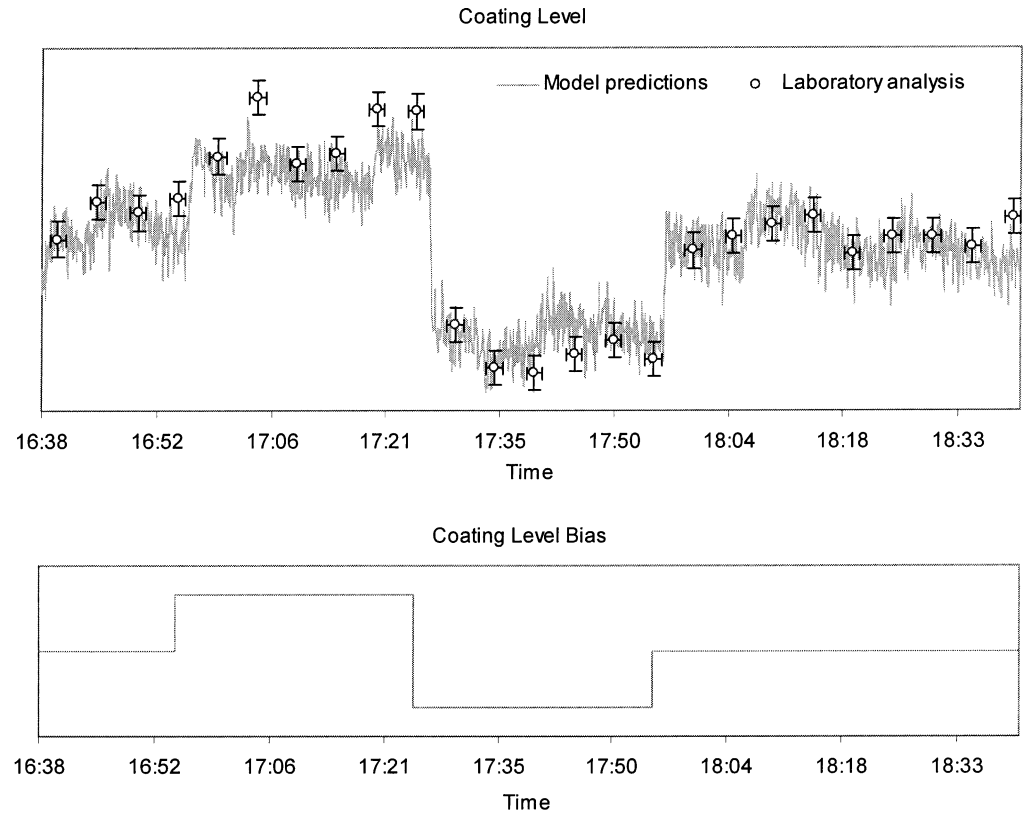


**Figure 10.** Open-loop experiment.

**4.2. Prediction of the Coating Level and Detection of the Hopper Effect on the Coating Level (Product A).** Some of the first data collected from the imaging system are shown in the upper plot in Figure 9. The raw coating predictions are shown by the light gray line. For this evaluation study, frequent grab samples were taken every 5 min and analyzed later in the laboratory. These are shown as circles in Figure 9. For each laboratory measurement, a $Y$ error bar and an $X$ error bar are also shown. The $Y$ error bar indicates the sampling and laboratory measure error (1 standard deviation) estimated from replicated sampling and analysis data. The $X$ error bar indicates the possible sample time mismatch between taking the digital images and manually grabbing the product sample for laboratory analysis. Here the error is estimated as $\pm 1$ min.

One can see that the predicted coating concentrations from the images are in good agreement with the

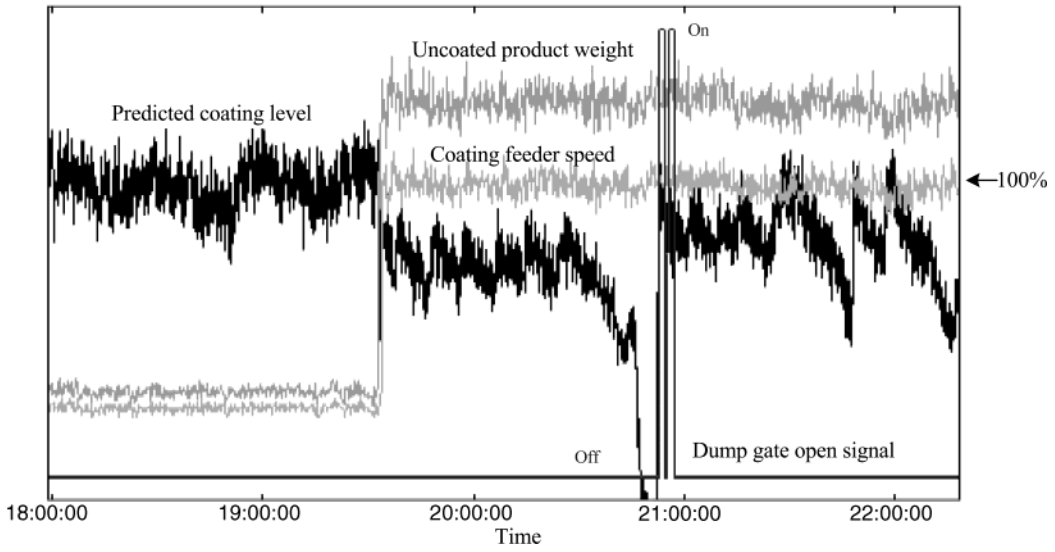


**Figure 11.** Online monitoring of product A.

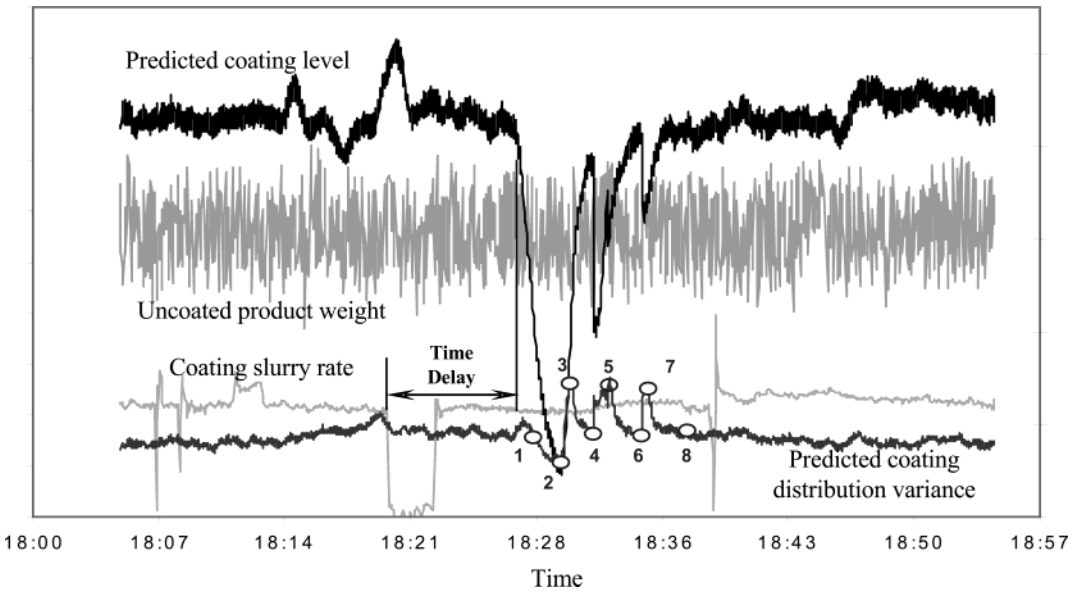


**Figure 12.** Online monitoring of product B.

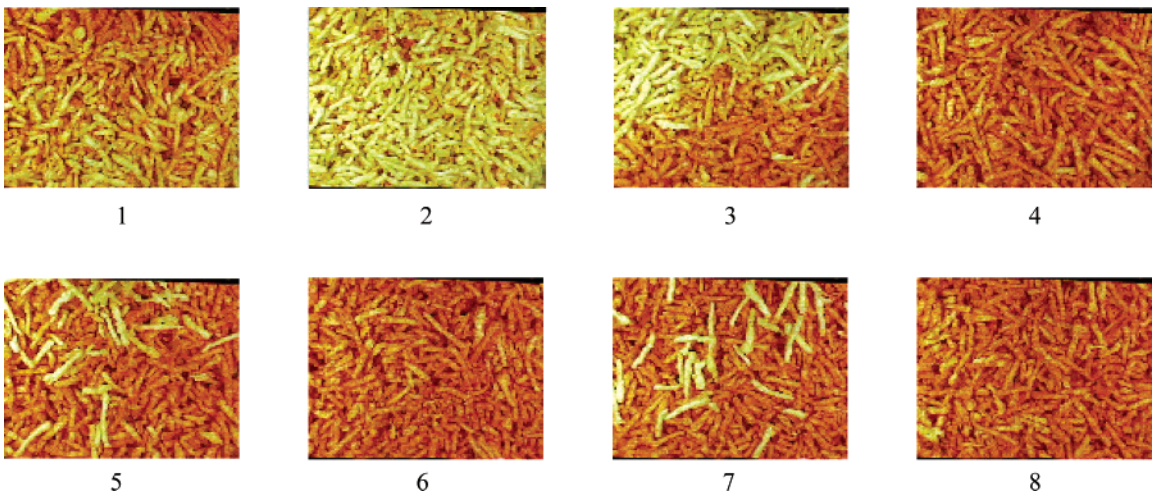


**Figure 13.** Images corresponding to the numbers marked in Figure 12.

laboratory analysis. However, the image predictions reveal a clear sawtooth behavior in the concentration that is not evident only from the laboratory data, even during this fast sampling program. This unexpected result was explained by the coating hopper refilling operations in the process. The lower plot in Figure 9

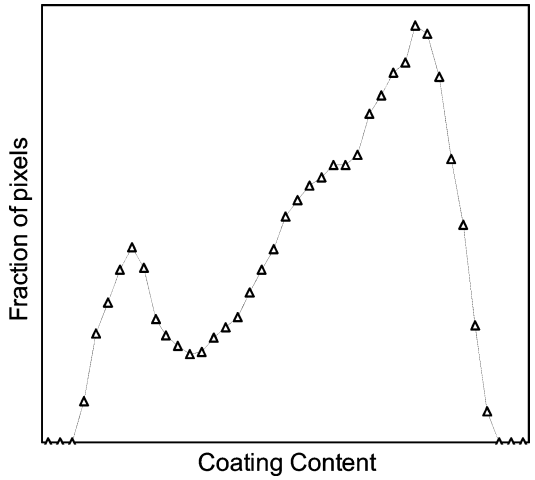


**Figure 14.** Coating distribution for image 5 in Figure 13 estimated using a small window strategy.

shows the signal of the motor of the hopper refilling system. As the level of the coating powder in the feed hopper falls to a certain level, the motor is activated to refill the hopper. The level of coating inside the hopper then increases rapidly. Clearly, Figure 9 shows that the discharge of the rate of coating from the hopper to the coating operation (tumbler) is a strong function of the coating level in the hopper.

**4.3. Open-Loop Experiment (Product A).** In Figure 10, the open-loop response of the coating level caused by changing the coating level bias (manipulated variable) is shown. The prediction and laboratory analysis coating levels are shown in the upper plot, and in the lower plot, the coating level bias signal is shown. Again we see that the predictions from the image analysis and the laboratory measurements are consistent. The predicted data show a clear fast response to each coating level bias change.

**4.4. Online Monitoring Examples (Products A and B).** Figure 11 shows a 4-h online monitoring period for product A. Shown are the predicted coating level, the uncoated product weight, the coating feeder speed, and the signal of the dump gate. During this period, at about time 19:35, the feed rate of the noncoated product to the tumbler suddenly increased and, as a result of ratio control, the coating feeder speed also increased. However, the coating feeder speed was limited by its maximum capacity and could not feed coating fast enough to keep the desired ratio to the uncoated product. Therefore, the coating level on the product decreased from the desired value. A second problem also occurred starting at about time 20:40, where the coating level suddenly started to continuously decrease. This occurred because the coating hopper was not set to automatic refilling mode and was therefore being depleted of coating. The result was that eventually no coating was being fed to the tumbler, and the dump gate had to be opened to remove the uncoated products from the belt. It should be pointed out that by looking only at process data (noncoated product weight and coating feeder speed) this fault was not detectable.

Figure 12 shows one example of online monitoring of both the coating concentration and the variance of the coating distribution for product B. In Figure 12 are shown the predicted coating level, the uncoated product weight, the coating slurry feed rate, and the predicted coating distribution variance. The variance of the coating distribution was calculated from the histogram of the coating concentrations obtained by applying the small window strategy outlined in section 3.5. During this approximate 1-h period of time, there was no large change in the feed rate of the uncoated product. However, we see that between time 18:19 and time 18:23 the coating slurry feed rate suddenly dropped to zero. The effect of this disturbance on the coated product appeared after about 8 min of time delay. At about time 18:27, both the predicted coating level and the coating distribution variance began to show large variation. To understand further what happened in the process during that time, Figure 13 shows eight images, corresponding to the eight numbers marked on the purple line in Figure 12. The predicted coating concentration drops off rapidly up to image 2 and then recovers in an irregular manner. The variance of the coating distribution decreases at image 2 because by this time most of the product is uniformly uncoated. During the subse-

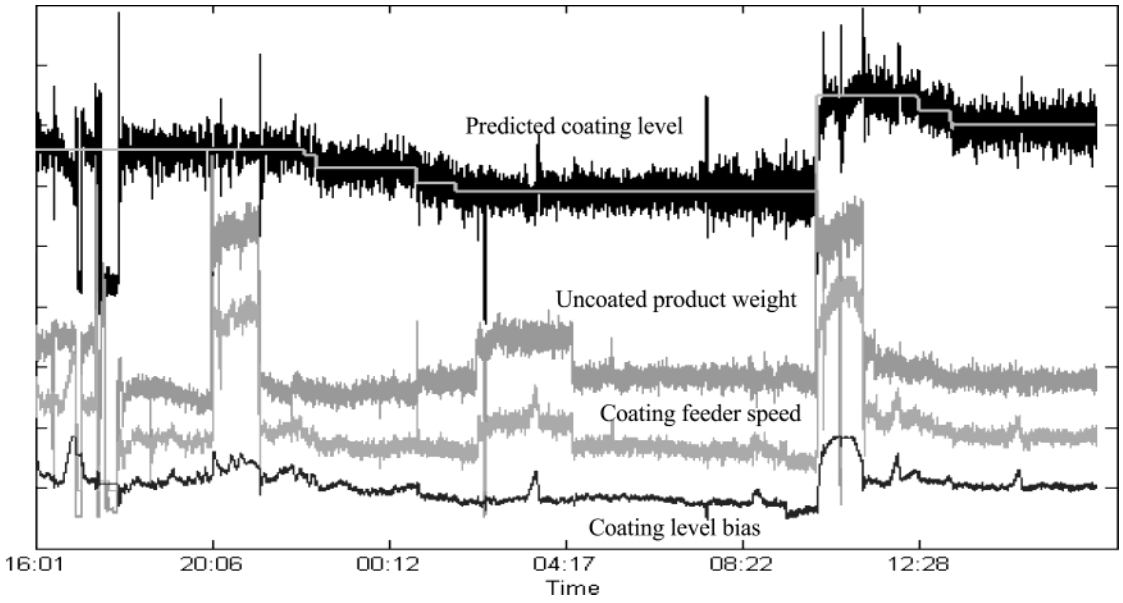


**Figure 15.** Closed-loop control for product A.

quent irregular recovery, shown in images 3−7 of Figure 13, the predicted variance of the coating distribution (Figure 12) is seen to vary widely as slugs of uncoated and coated product appear intermingled on the belt. The coating distribution plot (Figure 14) of image 5, as estimated from the small window strategy, shows a bimodal distribution as expected. Both the coating level and the coating variance appear to have recovered from the upset by image 8.

**4.5. Closed-Loop Control (Product A).** Finally, operating data under closed-loop control covering a period of 24 h are shown in Figure 15 for product A. Shown in the figure are the predicted coating level, the coating level set point (the light gray line through the predicted coating level), the uncoated product weight, the coating feeder speed, and the coating level bias change.

In the employed control scheme, the coating feeder speed is the manipulated variable and computed as the summation of the outputs of two controllers: a ratio controller for compensating variation of the uncoated product weight and a feedback controller. The coating level bias is the output of the feedback controller. From Figure 15, we can see that the coating level successfully tracked the set point. Another point to note from this figure is that we can no longer see the sawtooth effect of the coating feeder system that was apparent in Figures 9−11. This is because an operational change was introduced to eliminate this effect.

## 5. Conclusion

An online imaging system for monitoring and controlling product quality (coating concentration and distribution) has been developed and evaluated online on several industrial snack food processes. The results have been very successful.

The online imaging system has been used to successfully detect and diagnose problems in the plants that were not apparent without the almost instantaneous results available from the online images. The system is also being used to implement closed-loop control on the coating concentration.

## Literature Cited

(1) Ross, B. J.; Fueten, F.; Yashkir, D. Y. Automatic Mineral Identification Using Genetic Programming. *Mach. Vision Appl.* **2001**, *13*, 61.

(2) Stojanovic, R.; Mitropulos, P.; Koulamas, C.; Karayiannis, Y.; Koubias, S. Real-Time Vision-Based System for Textile Fabric Inspection. *Real-Time Imaging* **2001**, *7*, 507.

(3) Katafuchi, N.; Sano, M.; Ohara, S.; Okudaira, M. A Method for Inspecting Industrial Parts Surfaces Based on an Optics Model. *Mach. Vision Appl.* **2000**, *12*, 170.

(4) Esbensen, K.; Geladi, P. Strategy of Multivariate Image Analysis (MIA). *Chemom. Intell. Lab. Syst.* **1989**, *7*, 67.

(5) Esbensen, K.; Geladi, P.; Grahn, H. Strategies for Multivariate Image Regression (MIR). *Chemom. Intell. Lab. Syst.* **1992**, *14*, 357.

(6) Geladi, P.; Grahn, H. *Multivariate Image Analysis*; Wiley: New York, 1996.

(7) Bharati, M.; MacGregor, J. F. Multivariate Image Analysis for Real-Time Process Monitoring and Control. *Ind. Eng. Chem. Res.* **1998**, *37*, 4715.

(8) Bharati, M. Multivariate Image Analysis for Process Monitoring and Control. Ph.D. Thesis, 2002, McMaster University.

(9) Yu, H.; MacGregor, J. F. Multivariate Image Analysis and Regression for Prediction of Coating Content and Distribution in the Production of Snack Food. *Chemom. Intell. Lab. Syst.* **2002**, in press.

*Received for review* November 26, 2002
*Accepted* April 15, 2003

IE020941F